928 *Chem. Mater.* **2010,** *22,* 928–934
DOI:10.1021/cm901780z

CHEMISTRY OF MATERIALS
Article

Novel ZnO-Based Film with Double Light-Scattering Layers as Photoelectrodes for Enhanced Efficiency in Dye-Sensitized Solar Cells†

Yan-Zhen Zheng,[‡,§] Xia Tao,*[,‡] Li-Xin Wang,[‡] Hui Xu,[‡] Qian Hou,[‡] Wei-Lie Zhou,[∥] and Jian-Feng Chen*[,§]

[‡]*Key Laboratory for Nanomaterials of the Ministry of Education, Beijing University of Chemical Technology, Beijing 100029, China,* [§]*Research Center of the Ministry of Education for High Gravity Engineering & Technology, Beijing University of Chemical Technology, Beijing 100029, China, and* [∥]*Advanced Materials Research Institute, University of New Orleans, New Orleans, Louisiana 70148*

Received June 25, 2009. Revised Manuscript Received September 4, 2009

A novel double light-scattering-layer ZnO (DL-ZnO) film consisting of ZnO monodisperse aggregates (MA-ZnO) as underlayer and sub-micrometer-sized platelike ZnO (SP-ZnO) as overlayer was fabricated and studied as dye-sensitized solar-cell photoanodes. It was found that DL-ZnO could significantly improve the efficiency of dye-sensitized solar cells (DSSCs) owing to its relatively high surface area and enhanced light-scattering capability. The overall energy-conversion efficiency (η) of 3.44% was achieved by the formation of DL-ZnO film, which is 47% higher than that formed by MA-ZnO alone and far larger than that formed by SP-ZnO alone ($\eta = 0.81\%$). Furthermore, the η decay measurements for DL-ZnO cell showed that no significant decrease of η occurred even when DL-ZnO cell was placed for 100 h at ambient temperature. The charge recombination behavior of cells was investigated by electrochemical impedance spectra (EIS), and the results showed that among MA-ZnO, SP-ZnO, and DL-ZnO based cells, DL-ZnO based cell with double scattering layers has the lowest transfer resistance and the longest electron lifetime, which could facilitate the reduction of recombination processes and thus would promote the solar-cell performance.

Introduction

Dye-sensitized solar cells (DSSCs) have been found a wide practical application as an alternative to p−n junction solar cells because of their low fabrication cost and relatively high efficiency.[1−3] The primary photovoltaic (PV) material for DSSCs today is TiO_2, and TiO_2-based DSSCs have overcome the shortcomings of expensive cost associated with the construction of photovoltaic modules for solid-state devices. However, based on marketable options for the photovoltaic industry, the overall expense of synthesis, manufacture, processing, and device construction, as well as ultimate PV efficiency, must be considered.[1,4] Recently, ZnO-based DSSCs have attracted considerable interest because of their distinct advantages over the traditional TiO_2 in the aspects of high electron mobility (115−155 $cm^2\ V^{-1}\ s^{-1}$),[5] simple fabrication of the nanostructure and easy modification of the surface structure,[6,7] along with the similitude of band gap (3.37 eV) and electron-injection process to TiO_2,[4] however, overall solar-to-electric energy conversion efficiency (η) of ZnO-based cells is still relatively low. In recent years, more researchers have been focused on improving the efficiency of ZnO-based cells using nanostructured ZnO materials, especially ZnO one-dimensional materials (nanowires, nanorods, nanowire/nanorod arrays and nanotubes et al.), which are believed to gain the enhancement of efficiency because of their rapid electron transfer, reduction of charge recombination degree, and collection of carriers through electrical transport pathway.[8−15] However, the use of one-dimensional ZnO nanomaterials limits the surface area and interface of electrode films, resulting in a low η, for example, only

† Accepted as part of the 2010 "Materials Chemistry of Energy Conversion Special Issue".

*Corresponding author. E-mail: taoxia@yahoo.com (X.T.); chenjf@mail.buct.edu.cn (J.F.C.).

(1) O'Regan, B.; Grätzel, M. *Nature* **1991**, *353*, 737.
(2) Nazeeruddin, M. K.; Kay, A.; Rodicio, I.; Humphry-Baker, R.; Muller, E.; Liska, P.; Valchopoulos, N.; Grätzel, M. *J. Am. Chem. Soc.* **1993**, *115*, 6382.
(3) Hagfeldt, A.; Grätzel, M. *Chem. Rev.* **1995**, *95*, 49.
(4) Grätzel, M. *Nature* **2001**, *414*, 338.
(5) Kaidashev, E. M.; Lorenz, M.; Wenckstern, H.; von; Rahm, A.; Semmelhack, H. C.; Han, K. H.; Benndorf, G.; Bundesmann, C.; Hochmuth, H.; Grundmann, M. *Appl. Phys. Lett.* **2003**, *82*, 3901.
(6) Kakiuchi, K.; Hosono, E.; Fujihara, S. *J. Photochem. Photobiol. A* **2006**, *179*, 81.
(7) Zhang, T. R.; Dong, W. J.; Keeter-Brewer, M.; Konar, S.; Njabon, R. N.; Tian, Z. R. *J. Am. Chem. Soc.* **2006**, *128*, 10960.
(8) Law, M.; Greene, L. E.; Johnson, J. C.; Saykally, R.; Yang, P. D. *Nat. Mater.* **2005**, *4*, 455.
(9) Lee, Y. J.; Ruby, D. S.; Peters, D. W.; McKenzie, B. B.; Hsu, J.W. P. *Nano Lett.* **2008**, *8*, 1501.
(10) Hamann, T. W.; Martinson, A. B. F.; Elam, J. W.; Pellin, M. J.; Hupp, J. T. *Adv. Mater.* **2008**, *20*, 1560.
(11) Wang, K.; Chen, J. J.; Zhou, W. L.; Zhang, Y.; Yan, Y. F.; Pern, J.; Mascarenhas, A. *Adv. Mater.* **2008**, *20*, 3248.
(12) Gao, Y.; Nagai, M.; Chang, T.-C.; Shyue, J.-J. *Cryst. Growth Des.* **2007**, *7*, 2467.
(13) Guo, M.; Diao, P.; Wang, X.; Cai, S. M. *J. Solid State Chem.* **2005**, *178*, 3210.
(14) Guo, M.; Diao, P.; Cai, S. M. *Chin. Chem. Lett.* **2004**, *15*, 1113.
(15) Jiang, C. Y.; Sun, X. W.; Lo, G. Q.; Kwong, D. L.; Wang, J. X. *Appl. Phy. Lett.* **2007**, *90*, 263501.

 Published on Web 09/28/2009

2.4% for the nanowire/nanorod arrays[13] and 2.3% for the nanotube arrays.[14]

Alternatively, another effective method to the enhance efficiency in DSSCs is to build a light scattering layer with enhanced photocapture efficiency and optical absorption in photoelectrode films.[16−18] Following this strategy, submicrometer/micrometer-scale particles or pore-structured materials in the photoelectrode have been employed as light scattering objects based on the fact that optical absorption has been enhanced to a large extent when TiO_2 nanocrystalline films were combined with large particles.[19−22] Many scientists have succeeded in improving the η of TiO_2-based DSSCs by light-scatterer.[23−25] As for ZnO-based DSSCs, Fujihara et al.[26] fabricated micrometerano composite structured ZnO film by one-step self-assembly electrodeposition, with a η of 2.0%. Zhang et al.[27,28] have developed a new nanostructural ZnO nanocrystalline film consisting of monodisperse aggregates or polydisperse aggregates for the efficient adsorption of dye molecules and enhanced light absorption. In these systems, the light-scatter function is mainly originated from submicrometer-scale aggregates produced by the self-assembly of ZnO nanocrystalline particles. Indeed, introducing a monolayer moiety, fully composed of submicrometer-sized particles, into the electrode to build a bilayered composite film has also been proved to be effective in enhancing the efficiency of DSSCs.[23−25,29−31] To date, however, ZnO-based DSSCs with bilayer structure covering light-scattering overlayer and nanocrystalline underlayer has not been reported in the literature, which inspires us to develop a new bifunctional ZnO material with bilayer structure as photoelectrode for the enhancement of cell efficiency.

In this article, we report a significantly enhanced cell performance based on a double light-scattering-layer ZnO (DL-ZnO) structures composed of sub-micrometer-sized platelike ZnO (SP-ZnO) overlayer and ZnO monodispersed aggregates (MA-ZnO) underlayer. The single layer cells show moderate performance, whereas the double layer cells, fabricated through all-solution scale-up process, lead to coordinately improved characteristics including good optoelectric stability, low transfer resistance, and long electron lifetime. To the best of our knowledge, this is the first demonstration of such a bifunctional material consisting of ZnO nanocrystalline aggregates with large internal surface area for sufficient dye adsorption and double light-scattering layers containing sub-micrometer-sized ZnO aggregates and platelike particles for efficient photocapture and optical absorption.

Experimental Section

Materials. Anhydrous lithium iodide (LiI), iodide (I_2), tert-butyl pyridine (t-BPy), DMPII, acetonitrile, and H_2PtCl_6 were obtained from Sigma. Zinc acetate dihydrate [$(CH_3COO)_2Zn$], diethylene glycol [$(HOCH_2CH_2)_2O$], NaOH, HCl and ethanol (analytical grade purity) were purchased from Tianjin Chemical Reagents Co. and were used without further purification. N3 dye was obtained from Solaronix (Aubonne, Switzerland). All solutions used in this work were prepared with 18.2 MΩ cm^{-1} water produced by a reagent water system (Easy pure, Barnstead).

Preparation and Characterization of Uniform MA-ZnO and SP-ZnO Particles. SP-ZnO was synthesized by a hydrothermal process.[32] Briefly, 0.1 mol $(CH_3COO)_2Zn$ was mixed with 0.2 mol NaOH under stirring for 30 min. The pH value of the obtained solution was adjusted to 3 by diluted HCl solution. The above solution was transferred to Teflon-lined stainless steel autoclave, heated to 180 °C, and then kept for 10 h. The SP-ZnO product was obtained by filtration, rinsing with water to remove retained ions and impurities, and finally drying at 80 °C for 12 h. MA-ZnO was synthesized by the solvothermal process of zinc salt in polyol medium at 160 °C, similar to the method reported by Jezequel et al.[33] The typical synthesis procedure was described as follows: 0.02 mol [$(CH_3COO)_2Zn$] was added to $(HOCH_2CH_2)_2O$ and mixed with a magnetic stirring bar. The mixed solution was heated to 160 °C in an oil bath at a rate of 5 °C min^{-1} and then refluxed for 20 h. The as-prepared colloidal solution was then centrifuged at a rate of 5000 rpm for 10 min. The ZnO colloids precipitated at the bottom of the tubes were redispersed in ethanol by sonication for 20 min. This procedure of centrifugation and sonication was repeated several times in order to remove the supernatants. Finally, the resultant ZnO colloids were dispersed in 20 mL of ethanol and sealed at room temperature in stock.

The morphology of the as-synthesized MA-ZnO and SP-ZnO particles was characterized by field emission scanning electron microscope (FE-SEM, JEOL, JSM 6701-F). High-resolution transmission electron microscopy (HR-TEM) images were recorded on a JEOL JEM-3010 microscope. Prior to X-ray diffraction (XRD) and Brunauer−Emmett−Teller (BET) measurements MA-ZnO colloides and SP-ZnO powder were dried at 100 °C for 12 h. XRD data were obtained using an X-ray diffractometer (Rigaku, D/max 2500 VB2+/PC), in 2θ range from 10° to 80° with Cu Kα radiation ($\lambda = 0.15406$ nm) operated

(16) Ferber, J.; Luther, J. *Sol. Energy Mater. Sol. Cells* **1998**, *54*, 265.
(17) Usami, A. *Chem. Phys. Lett.* **1997**, *277*, 105.
(18) Rothenberger, G.; Comte, P.; Grätzel, M. *Sol. Energy Mater. Sol. Cells* **1999**, *58*, 321.
(19) Hore, S.; Nitz, P.; Vetter, C.; Prahl, C.; Niggemann, M.; Kern, R. *Chem.Commun.* **2005**, *15*, 2011.
(20) Anderson, C.; Bard, A. J. *J. Phys. Chem. B* **1997**, *101*, 2611.
(21) Barbe, C. J.; Arendse, F.; Comte, P.; Jirousek, M.; Lenzmann, F.; Shklover, V.; Grätzel, M. *J. Am. Ceram. Soc.* **1997**, *80*, 3157.
(22) So, W. W.; Kim, K. J.; Lee, J. K.; Moon, S. J. *Jpn. J.Appl. Phys. Part 1* **2004**, *43*, 1231.
(23) Nishimura, S.; Abrams, N.; Lewis, B. A.; Halaoui, L. I.; Mallouk, T. E.; Benkstein, K. D.; Lagemaat, J. van de; Frank, A. J. *J. Am. Chem. Soc.* **2003**, *125*, 6306.
(24) Koo, H. J.; Kim, Y. J.; Lee, Y. H.; Lee, W. I.; Kim, K.; Park, N. G. *Adv. Mater.* **2008**, *20*, 195.
(25) Halaoui, L. I.; Abrams, N. M.; Mallouk, T. E. *J. Phys. Chem. B* **2005**, *109*, 6334.
(26) Hosono, E.; Fujihara, S.; Kimura, T. *Electrochim. Acta* **2004**, *49*, 2287.
(27) Zhang, Q. F.; Chou, T. P.; Russo, B.; Jenekhe, S. A.; Cao, G. Z. *Adv. Funct. Mater.* **2008**, *18*, 1654.
(28) Chou, T. P.; Zhang, Q. F.; Fryxell, G. E.; Cao, G. Z. *Adv. Mater.* **2007**, *19*, 2588.
(29) Wang, Z.-S.; Kawauchi, H.; Kashima, T.; Arakawa, H. *Coord. Chem. Rev.* **2004**, *248*, 1381.
(30) Ito, S.; Zakeeruddin, S. M.; Humphry-Baker, R.; Liska, P.; Charvet, P.; Comte, P.; Nazeeruddin, M. K.; Péchy, P.; Takata, M.; Miura, H.; Uchida, S.; Grätzel, M. *Adv. Mater.* **2006**, *18*, 1202.
(31) Hore, S.; Vetter, C.; Kern, R.; Smit, H.; Hinsch, A. *Sol. Energy Mater. Sol. Cells* **2006**, *90*, 1176.
(32) Chen, D. R.; Jiao, X. L.; Cheng, C. *Solid State Commun.* **2000**, *113*, 363.
(33) Jezequel, D.; Guenot, J.; Jouini, N.; Fievet, F. J. *Mater. Res.* **1995**, *10*, 77.

at 40 mA and 40 kV. An ASAP 2010 surface area analyzer was used to determine BET data of the MA-ZnO and SP-ZnO samples.

Preparation and the Morphology Characterization of ZnO Electrode Films. Fluorine-doped tin oxide-coated glass (FTO, Hartford, 14 Ω/sq, 80% transmittance) plates were used as the substrates. Before fabricating ZnO film, the FTO substrates were ultrasonically cleaned sequentially in HCl, acetone, ethanol and water each for 15 min and dried at the atmosphere of Ar. A few drops of the resultant ZnO colloids were dripped onto the FTO substrates using drop-coat method to construct the photoelectrode films. After being dried, a milk white ZnO nanocrystalline aggregate film was formed by annealing at 350 °C for 60 min, accompanied by evaporation of residual organic solvent from the ZnO surface. The composite DL-ZnO film with bilayer structure was constructed by coating the as-prepared SP-ZnO particles on the above-mentioned ZnO nanocrystalline aggregate film and then heating at 350 °C for 60 min. Simultaneously, we prepared a monolayer film consisting of MA-ZnO only or SP-ZnO only under identical experimental condition as described for the DL-ZnO film. Usually, the thickness of films was controlled by the concentration of ZnO in ethanol. For comparison, the thickness of single MA-ZnO film and single SP-ZnO film was also experimentally controlled to be identical to that of DL-ZnO film. The surface morphology of the ZnO nanocrystallite film was investigated by FESEM (Hitachi S-4700 and JEOL, JSM 6701-F) operated at 20 kV.

Dye Adsorption and Dye Loading Measurement of ZnO Electrode Films. Prior to solar cell testing, the resulting ZnO films were heated at 70 °C for 30 min and dye-loading of ZnO films was performed by immersing in a 0.5 mM ethanolic solution of the ruthenium complex cis-$[RuL_2(NCS)_2]$ (commercially called as N3 dye) for approximately 30 min at room temperature. The sensitized films were rinsed with ethanol to remove excess dye remaining on the surface and then air-dried at room temperature. In order to measure the concentration of dye in ZnO electrode, the dye was desorbed into a 1.0 M NaOH solution in water/ethanol (50:50, V/V) and absorption spectrum of the desorbed-dye solution was detected using a UV−vis spectrophotometer (UV 2501 spectrometer, Shimadzu).[34,35]

Cell Assembly and Characterization. Counter electrodes were prepared by depositing a platinum thin film on the FTO glass with a hole using 0.35 mM H_2PtCl_6 solution, followed by annealing at 400 °C for 15 min in air. Pt electrodes were placed over the dye-adsorbed ZnO electrodes and the edges of the solar cells were sealed with 2 mm wide stripes of sealing sheet (Parafilm, Pechiney Plastic Packaging Inc.). For solar cell assembly, hot-pressing methods were performed at 80 °C for 1−2 min. Subsequently, the electrolyte solution, consisting of 0.3 M LiI, 0.06 M I_2, 0.5 M *t*-BPy and 1.0 M DMPII in acetonitrile, was injected into the cell through the small hole drilled in the Pt counter electrode. The hole was then covered and sealed with a small square glass sealing sheet to prevent electrolyte leakage. During the assembly procedures, the active area of the resulting cell exposed in light was approximately 1.0 cm^2 (1 cm × 1 cm).

The photoelectrochemical tests of DSSCs were performed under one sun condition using a solar light simulator (Oriel, 69911, AM 1.5 globe) with 100 mW cm^{-2} light output. The photocurrent−voltage characteristics and the electrochemical impedance spectroscopy (EIS) measurements of all the DSSCs were performed using electrochemical workstation (CHI660C, ShangHai) under 100 mW cm^{-2}. The open circuit voltage (V_{oc}) was defined at $I = 0$, and the short-circuit current (J_{sc}) was set at $V = 0$. The frequency range was explored from 0.1 Hz to 100 kHz, and the applied bias voltage and ac amplitude were set at open-circuit voltage of the DSSCs and 10 mV between the FTO-Pt counter electrode and the FTO-ZnO-dye working electrode, respectively.[36] The ac impedance spectra were analyzed by an equivalent circuit model for interpreting the characteristic of the DSSCs.[37] Monochromatic light in the range of 400−800 nm was obtained by using a series of filters. The incident photo to current conversion efficiency (IPCE) was measured as a function of wavelength from 400 to 800 nm on a Keithley model 2000 SourceMeter under short circuit conditions using a tungsten source.

Results and Discussion

Morphological Characterization of ZnO Electrode Films. Figure 1a and 1b show the FESEM images of self-made MA-ZnO and SP-ZnO particles. MA-ZnO particles in shape are ∼250 nm sized spheres. One can see that ZnO aggregates are composed of packed ZnO nanocrystallite particles with the diameter of 15−20 nm. SP-ZnO particles appear as flattened plate with 100−500 nm in diameter. The HRTEM image of SP-ZnO particles (shown in Figure1c) reveals that the SP-ZnO is single-crystalline in wurtzite crystal structure and the lattice fringe of $d = 0.26$ nm, corresponding to the (002) plane of the hexagonal ZnO, implying the growth along *c*-axis for the ZnO plates The inset is fast Fourier transform (FFT) pattern of SP-ZnO particles from Figure1c and shows the (002) diffraction spots. The crystallinty of MA-ZnO and SP-ZnO samples were analyzed by XRD patterns (see Figure 1d). All the peaks are indexed to be wurtzite hexagonal-shaped ZnO with space group $P6_3mc$ (Joint Committee on Powder Diffraction Standards (JCPDS) card file 36−1451), corresponding to (100), (002), (101), (102), (110) and (103) planes of ZnO. The BET surface areas for MA-ZnO and SP-ZnO are determined to be 51 and 7 $m^2\ g^{-1}$, respectively. All data and analytic results of Figure 1 are summarized in Table 1.

The double-layer ZnO film was prepared by in sequence drop-coating ZnO nanocrystalline aggregates and platelike ZnO particles on FTO substrate. Figure 2a depicts the schematic diagram of the ZnO film with bilayer structure. A cross-sectional FESEM image provides a direct observation on bilayer texture structure of as-prepared film, i.e., containing a 1.5 μm thick SP-ZnO overlayer and a 3 μm thick MA-ZnO particulate underlayer (see Figure 2b). Images c and d in Figure 2 show FESEM images (top views) of MA-ZnO underlayer and SP-ZnO overlayer films, respectively, in which Figure 2c was examined immediately after MA-ZnO underlayer

(34) Wang, Z. S.; Kawauchi, H.; Kashima, T.; Arakama, H. *Coord. Chem. Rev.* **2004**, *248*, 1381.
(35) Zhao, D.; Peng, T.; Lu, L.; Cai, P.; Jiang, P.; Bian, Z. *J. Phys. Chem. C* **2008**, *112*, 8486.
(36) Longo, C.; Freitas, J.; De Paoli, M. A. *J. Photochem. Photobiol. A: Chem.* **2003**, *159*, 33.
(37) Bernard, M. C.; Cachet, H.; Falaras, P.; Hugot-Le Goff, A.; Kalbac, M.; Lukes, I.; Oanh, N. T.; Stergiopoulos, T.; Arabatzis, I. *J. Electrochem. Soc.* **2003**, *150*, E155.

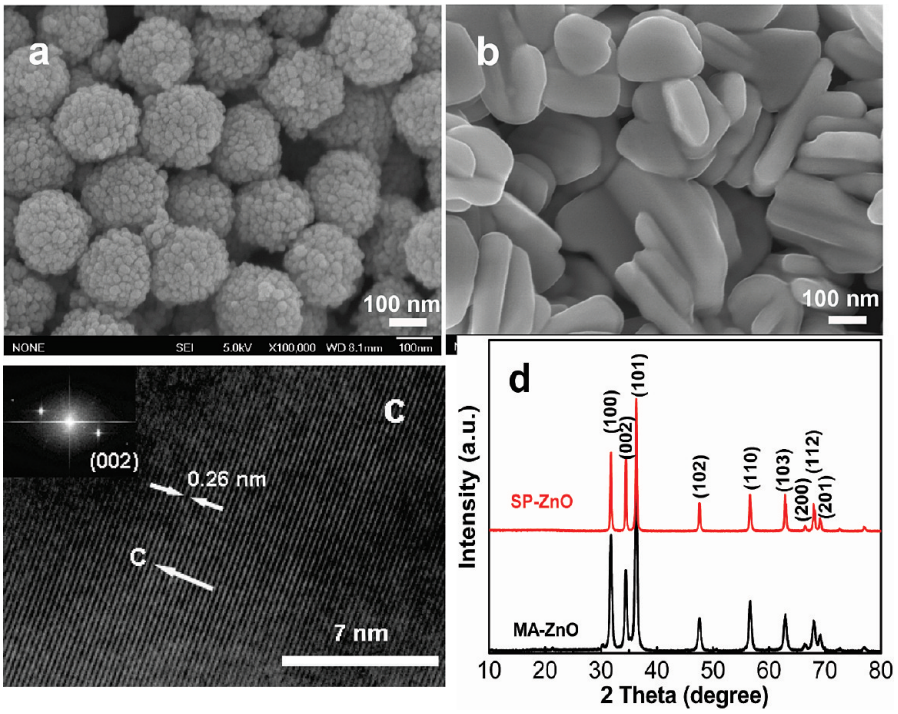

Figure 1. FESEM images of as-prepared (a) MA-ZnO and (b) SP-ZnO. (c) HRTEM image of SP-ZnO, with its corresponding FFT pattern for the ZnO plate in the wurtzite phase grown along the [0001] direction with *d*-spacing of 0.26 nm. (d) XRD patterns for MA-ZnO and SP-ZnO.

Table 1. Physical Parameters of MA-ZnO and SP-ZnO Particles

ZnO materials	S_{BET}[a] (m^2/g)	shape	size (nm)	cryst structure	cryst syst	space group
MA-ZnO	51	sphere[b]	~250	Wurtzite	hexagonal	$P6_3mc$
SP-ZnO	7	plate	100−500	Wurtzite	hexagonal	$P6_3mc$

[a] Data are obtained from adsorption isotherms of nitrogen at 30 °C. [b] The MA-ZnO is shaped with ~250 nm diameter hierarchical spheres made up of 15−20 nm diameter nanoparticles.

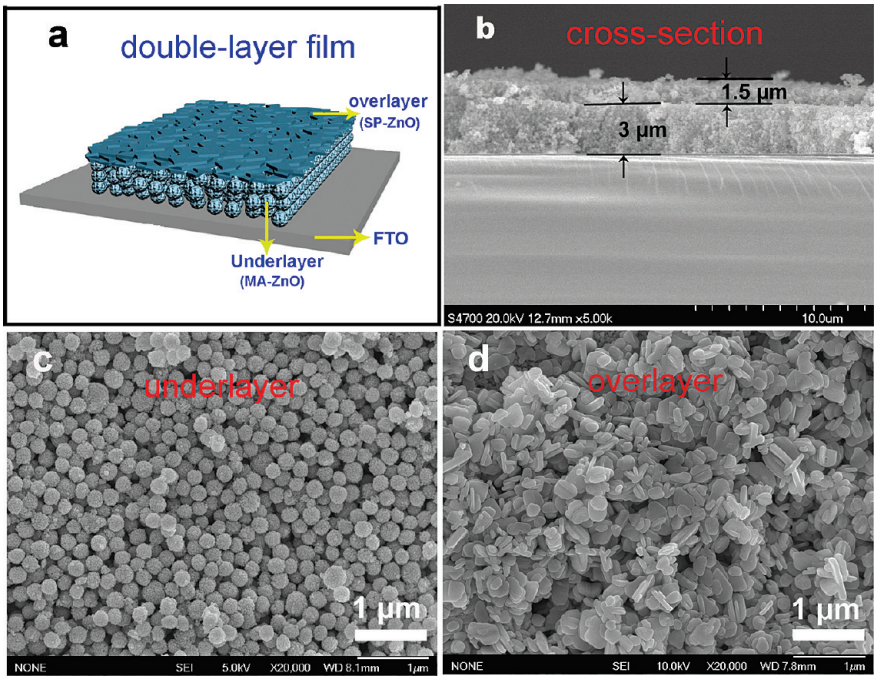

Figure 2. (a) Scheme of ZnO film based on double-layer structure; (b) FESEM image showing a cross-section of a bilayer-structural ZnO photoelectrode film (thickness is indicated for MA-ZnO underlayer and SP-ZnO overlayer, respectively); and surface FESEM images for (c) SP-ZnO overlayer and (d) MA-ZnO underlayer. Scale bars are 10, 1, and 1 μm for b−d, respectively.

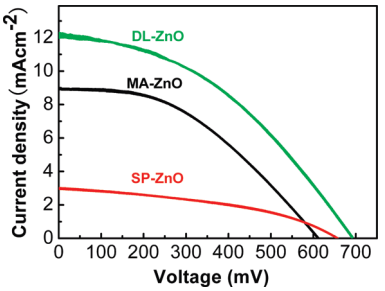

Figure 3. Photocurrent density−voltage curves of DSSCs based on MA-ZnO, SP-ZnO, and DL-ZnO, respectively.

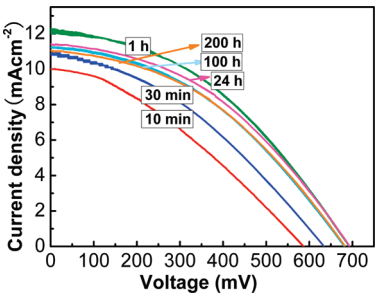

Figure 4. $I-V$ curves of the DL-ZnO cell measured repeated at various time intervals including 10 min, 30 min, 1 h, 24 h, 100 h, and 200 h.

Table 2. Comparison of *Jsc*, *Voc*, *FF*, and η together with the Amount of Adsorbed N3 Dye for DSSCs for MA-ZnO, SP-ZnO, and DL-ZnO Films

samples	*Jsc* (mA/cm^2)	*Voc* (mV)	*FF*	η (%)	adsorbed dye ($\times 10^{-8}$ mol cm^{-2})[a]
MA-ZnO	8.96	612	0.43	2.34	4.44
SP-ZnO	3.01	657	0.41	0.81	0.86
DL-ZnO	12.30	692	0.41	3.44	3.66

[a] Dye-adsorbed films with a dimension of 4 cm^2 were used for estimating the adsorbed dye concentration. The total amount of dye measured by UV−vis absorption was divided by the film area.

formed and annealed, and Figure 2d was captured after DL-ZnO film formed and annealed. The underlayer of DL-ZnO film is well stacked with hierarchically structured ~250 nm-sized ZnO monodisperse aggregates, which was constructed by the random agglomeration of tiny 15−20 nm sized ZnO nanocrystalline particles. The light-scattering overlayer was made of 100−500 nm sized ZnO plates. It is worth mentioning that the adhesion property between MA-ZnO underlayer and SP-ZnO overlayer interfaces in DL-ZnO films remains relatively strong because no scraps or fragments fallen from film after annealing were observed.

PV Performance of ZnO-Based DSSCs. The photocurrent density−photovoltaic performance for DSSCs based on MA-ZnO, SP-ZnO, and DL-ZnO under the AM1.5 sunlight illumination (100 mW/cm^2) is displayed in Figure 3. Table 2 summarizes the measured and calculated values obtained from the typical $I-V$ curve (Figure 3). It can be seen that the J_{sc} and η of DL-ZnO film were obviously higher than that of MA-ZnO or SP-ZnO film. MA-ZnO cell exhibited a J_{sc} value of 8.96 mA/cm^2, whereas its V_{oc} value was 612 mV. According to the current−voltage curve of MA-ZnO film, a fill factor (FF) of 0.43 and a η value of 2.34% were obtained for this cell, which was similar to η value of 1.5−2.3% for the films with 160−300 nm monodisperse aggregation of ZnO nanocrystallites (see ref 18). For SP-ZnO DSSC, a η value of only 0.81% was obtained. When SP-ZnO particles were introduced as an overlayer, however, the J_{sc} value of the fabricated DL-ZnO DSSC increased to 12.30 mA/cm^2 and η enhanced up to 3.44%. This η value corresponds to a 47% increment of MA-ZnO DSSC and is much larger than that of SP-ZnO DSSC. It is worth mentioning that the relative thickness ratio of SP-ZnO to MA-ZnO used here was 1.5: 3 and the thickness of all ZnO films involved was ~4.5 μm as a whole. We have also

Table 3. Decay Test Data of DL-ZnO Cell Measured Repeated at Various Time Intervals Including 10 min, 30 min, 1 h, 24 h, 100 h, and 200 h

time intervals	*Jsc* (mA/cm^2)	*Voc* (mV)	*FF*	η (%)
10 min	10.00	587	0.34	2.01
30 min	10.90	634	0.37	2.54
1 h	12.30	692	0.41	3.44
24 h	11.41	693	0.41	3.26
100 h	11.22	682	0.40	3.08
200 h	11.05	682	0.41	3.08

systematically studied the effect of thickness ratio on photovoltaic performance of DL-ZnO cell as shown in Table S1 of the Supporting Information. It was found that 1.5: 3 of SP-ZnO to MA-ZnO thickness results in the maximum efficiency among a series of thickness ratios of 1:3.5, 1.3 3.2, 1.5:3, 1.8:2.7, and 2:2.5. Thus, in the following measurements, the optimized thickness ratio, i.e., 1.5:3, was adopted for the DL-ZnO film.

To further examine the photovoltaic performance of DL-ZnO based DSSCs, we carried out the decay test. The $I-V$ measurement of this cell was monitored repeatedly at different time interval and the results are shown in Figure 4. Within the initial period of 1 h, V_{oc} increases from 587 mV up to the maximum value of 692 mV, accompanied by the increase of J_{sc} from 10.00 to 12.30 mA/cm^2. Afterward, with prolonged test time ranging from 1 to 200 h, the J_{sc} and the V_{oc} decrease slightly (from 12.30 to 11.05 mA/cm^2 for J_{sc} and from 692 to 682 mV for V_{oc}). The first increased behavior is understandable because the fully contact between the electrolyte and ZnO (or N3) needs a durative soakage period, i.e., ca. 1 h, for achieving high J_{sc} and η. With the increase in test time, irreversible intercalated Li ions could occur and gradually accumulate in the photoelectrode film and hence lead to the decrease in J_{sc} and η.[38,39] Obviously, after placing for 1 h at ambient temperature, the η of the DL-ZnO-based cell reaches up to a maximum value of 3.44% based on the highest J_{sc} and V_{oc} during the whole test time of 200 h. All decay test data for the DL-ZnO cell are summarized in Table 3. It is worth noting that within the period of 1−200 h, only 10% degradation of J_{sc} was observed, which is superior to that of mesoporous nanosheet ZnO cell with a decay value of J_{sc} from 7.9 to 5.2 mA/cm^2.[40] Although we for the moment cannot comment on the enhanced performance of DL-ZnO

(38) Kang, S. H.; Lim, J.-W.; Kim, H. S.; Kim, J.-Y.; Chung, Y.-H.; Sung, Y.-E. *Chem. Mater.* **2009**, *21*, 2777.
(39) Janke, N.; Bieberle, A. *Thin Solid Films* **2001**, *392*, 134.
(40) Kakiuchi, K.; Saito, M.; Fujihara, S. *Thin Solid Films* **2008**, *516*, 2026.

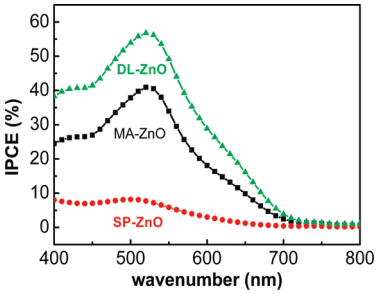

Figure 5. IPCE spectra of DSSCs based on MA-ZnO, SP-ZnO, and DL-ZnO.

cell in terms of decay compared with mesoporous nanosheet ZnO cell, the inherent structural nature of the DL-ZnO photoanode film constructed by SP-ZnO particles and MA-ZnO aggregates, together with the multiporous network structure cross-linked among the particles, could be assumed as a possible explanation.

The photocurrent action spectra of the cells are shown in Figure 5, which displays IPCE spectra as a function of wavelength for MA-ZnO-, SP-ZnO-, and DL-ZnO-based DSSCs. The DL-ZnO-based cell shows a better photoelectrical response, and its absolute IPCE is obviously higher than that of MA-ZnO and SP-ZnO over the entire wavelength region of 400−800 nm. This is also in good agreement with the observed higher J_{sc} of DL-ZnO cell as displayed in Figure 3. The maxima of IPCE contributed by the N3 dye absorption at approximately 520 nm in the visible region are 41% for MA-ZnO cell, 8% for SP-ZnO cell, and 57% for DL-ZnO cell, respectively. Detailed explanation for the enhancement of IPCE of DL-ZnO cell will be further discussed later.

EIS Analyses. EIS technique has been widely employed to investigate the kinetics of electrochemical and photoelectrochemical process occurring in DSSCs, lithium cell and supercapacitor.[41−47] The impedance spectra of DSSCs based on MA-ZnO, SP-ZnO, and DL-ZnO under illumination were measured ranging from 0.1 Hz to 100 kHz at the V_{oc}, with values of 612, 657, and 692 mV, respectively, as illustrated in Figure 6.

Two semicircles, including a small one at high frequency and a large semicircle at low frequency, were observed in the Nyquist plots of EIS spectra (see Figure 6a). As can be seen, the small semicircle in the frequency range (<0.1 MΩ) fitted to a charge-transfer resistance (R_{ct}) and the chemical capacitance ($C\mu$) should be ascribed to the charge transfer at the interfaces of the

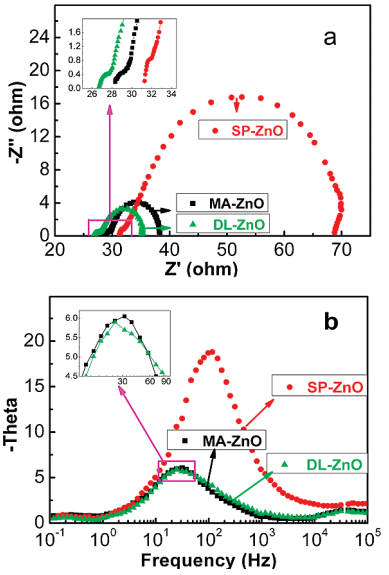

Figure 6. EIS spectra of MA-ZnO-, SP-ZnO-, and DL-ZnO-based DSSCs. (a) Nyquist plots, in which the inset is a magnified profile of selected rectangle area in high-frequency region; (b) Bode phase plots, in which the inset is a magnified profile of selected rectangle area in low-frequency peak region. Conditions: open-circuit, 100 mW cm^{-2} simulated light.

Table 4. Kinetic Parameters of the Recombination Reaction within MA-ZnO-, SP-ZnO-, and DL-ZnO-Based DSSCs

samples	R_{ct} (Ω)	R_w (Ω)	τ_e (ms)
MA-ZnO	7.71	9.31	5.06
SP-ZnO	29.95	10.11	1.42
DL-ZnO	5.53	3.36	6.45

redox electrolyte/Pt counter electrode.[41,43] The large semicircle in the low-frequency region fitted to a transport resistance (R_w) and a constant phase element (Q) is related to the accumulation/transport of the injected electrons within ZnO film and the charge transfer across either the ZnO/redox electrolyte interface or the FTO/ZnO interface. According to the EIS model reported in the literature,[41,43] the fitted parameters including Rct and Rw obtained by Zsimpwin software are exhibited in Table 4. From the Table 4, one can see that DL-ZnO system exhibits the lowest values for Rct and Rw resistance among three cells, implying that more efficient charge-transfer process at the dye-coated DL-ZnO/electrolyte interface and the Pt counter electrode/redox electrolyte interface occurs. The Bode phase plots of EIS spectra, as shown in Figure 6b, display the frequency peaks of the charge transfer process at different interfaces for three kinds of ZnO-based cells. The characteristic low-frequency peaks (f_{max}) are located at 117.0 Hz for SP-ZnO cell, 35.1 Hz for MA-ZnO cell, and 27.4 Hz for the DL-ZnO cell, repectively. The electron lifetime for recombination (τ_e) in ZnO- based DSSCs is determined by f_{max} values, where $\tau_e = 1/\omega_{min} = 1/2\pi f_{max}$.[41,43] An increased trend of τ_e in a sequence of SP-ZnO < MA-ZnO < DL-ZnO cells was observed in Table 4. The low resistance and long electron lifetime could favor the electron transport through a longer distance with less diffusive hindrance to some extent, and thus probably leading to the reduction

(41) Lagemaat, J. van de; Park, N.-G.; Frank, A. J. *J. Phys. Chem. B* **2000**, *104*, 2044.
(42) Longo, C.; Nogueira, A. F.; De Paoli, M.-A.; Cachet, H. *J. Phys. Chem. B* **2002**, *106*, 5925.
(43) Papageorgiou, N.; Maier, W. F.; Grätzel, M. *J. Electrochem. Soc.* **1997**, *144*, 876.
(44) Wang, Q.; Moser, J.-E.; Grätzel, M. *J. Phys. Chem. B* **2005**, *109*, 14945.
(45) Han, L.; Koide, N.; Chiba, Y.; Mitate, T. *Appl. Phys. Lett.* **2004**, *84*, 2433.
(46) Zhao, Y.; Zhai, J.; He, J. L.; Chen, X.; Chen, L.; Zhang, L. B.; Tian, Y. X.; Jiang, L.; Zhu, D. B. *Chem. Mater.* **2008**, *20*, 6022.
(47) Zheng, Y. Z.; Ding, H. Y.; Zhang, M. L. *Thin Solid Films* **2008**, *516*, 7381.

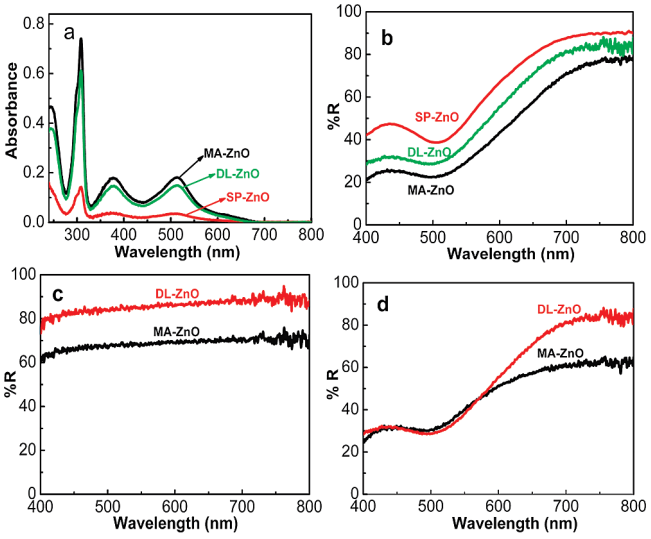

Figure 7. (a) Optical absorption and (b) diffused reflectance spectra of MA-ZnO, SP-ZnO, and DL-ZnO films with adsorbed N3 dye; and diffused reflectance spectra of MA-ZnO film (3 μm) and DL-ZnO (4.5 μm) film (c) without and (d) with adsorbed N3 dye.

of electron recombination and the capture of more effective electrons.[48−52]

UV Absorption and Reflectance Spectra Measurements. The more dye adsorption amount and enhanced light scattering effect are considered to be two main influence factors to increase the efficiency of DSSCs.[24] UV/vis absorption spectra of N3 dye in MA-ZnO, SP-ZnO and DL-ZnO films are displayed in Figure 7a and the dye adsorption amount in the three ZnO films is exhibited in Table 2. Obviously, the adsorbed amount of dye in DL-ZnO film (3.66×10^{-8} mol cm^{-2}) is slightly lower than that in MA-ZnO film (4.44×10^{-8} mol cm^{-2}), and much higher than that in SP-ZnO film (0.86×10^{-8} mol cm^{-2}). This is understandable because the surface area of MA-ZnO particles is greater than that of SP-ZnO samples (see Table 1), which facilitates more amounts of dye molecules adsorbed in the films with MA-ZnO particles. As for DL-ZnO film, one would imagine that the effective surface area is slightly reduced after covering the SP-ZnO on the top surface of the MA-ZnO, resulting in a reduced N3, which also accords with N3 absorption spectra data, that is, DL-ZnO exhibits the relatively lower absorption peak height compared with MA-ZnO (see Figure 7a). The reflectance spectra of three ZnO films were also examined in the work. From Figure 7b one can see that the DL-ZnO film exhibits an apparently higher reflectance than the MA-ZnO film, but is lower than SP-ZnO film, indicating that the large particles with plate-like structure have a higher-scattering ability than those in two other kinds of films with large aggregates assembled with nanocrystalline particles. To further verify double-light scattering of DL-ZnO film with bilayer structure, we also sequentially prepared a 3 μm MA-ZnO film and a 4.5 μm DL-ZnO film composed of 3 μm MA-ZnO underlayer and 1.5 μm SP-ZnO overlayer. The R% spectra of the two fabricated films before and after N3 adsorption were separately examined and the results were displayed in panels c and d in Figure 7. As shown in Figure 7c, prior to N3 adsorption the reflectance of the DL-ZnO film (80−90%) is higher than that of MA-ZnO film (60−70%). After adsorbing N3 (Figure 7d), the two dye-adsorbed films, analogous to the reflectance without N3 adsorption, still possess good reflectance performance in the long wavelength region ranging from 600−800 nm. These results indicate that DL-ZnO film has offered greatly double-light scattering. Additionally, an obvious reflectance decrease in the short wavelength region of 400−600 nm could be mainly attributed to light absorption by dye molecules.[24] Considering the synergic effect of relatively high dye absorption amount and great light scattering in the DL-ZnO photoelectrode, the DL-ZnO-based cell exhibits the highest η and IPCE among the three cells studied.

Conclusion

We have succeessfully fabricated DL-ZnO film consisting of 100−500 nm sized SP-ZnO films as an overlayer and a ~250 nm MA-ZnO composed of 15−20 nm sized nanocrystalline particles as an underlayer to promote solar-cell performance. The bilayer light-scattering electrode film was confirmed to possess bifunctional characters, i.e., efficient light scattering and light absorption. The photovoltaic measurement results showed that the η of DL-ZnO cell is enhanced and reached up to a maximum value of 3.44% upon being tested at time interval of 1 h at ambient temperature. The decay test demonstrated that DL-ZnO cell had relatively stable photoelectrochemical property. Compared with monolayered MA-ZnO and SP-ZnO cells, the DL-ZnO-based cell with double scattering layers has the lowest transfer resistance and the longest electron lifetime under simulated solar illumination via EIS data analyses, which could facilitate the reduction of recombination processes and lead to the capture of more electrons. Thus, double light-scattering layers and effective light absorption of nanocrystalline applied in DSSCs open up a new route to the fabrication of low-cost, environmentally safe, and durable materials with excellent solar-to-electric efficiency.

Acknowledgment. This work was supported financially by NSFC (20776014, 20906004, 20977005, 20821004), CPSF (20080440303), 863 project (2007AA03Z343), the Key Program for Science and Technology Research from the ministry of education of China (107009), and the NCET project (NCET-06-0102).

Supporting Information Available: Characterization information and Table S1 (PDF). This material is available free of charge via the Internet at http://pubs.acs.org.

(48) Qian, J.; Liu, P.; Xiao, Y.; Jiang, Y.; Cao, Y.; Ai, X.; Yang, H. *Adv. Mater.* **2009**No. DOI:10.1002/adma.200900525.
(49) Kim, Y. J.; Lee, M. H.; Kim, H. J.; Lim, G.; Choi, Y. S.; Park, N.-G.; Kim, K.; Lee, W. I. *Adv. Mater.* **2009**No. DOI:10.1002/adma.200900294.
(50) Kwak, E. S.; Lee, W.; Park, N.-G.; Kim, J. H.; Lee, H. *Adv. Funct. Mater.* **2009**, *19*, 1093.
(51) Zhang, Q.; Dandeneau, C. S.; Zhou, X.; Cao, G. *Adv. Mater.* **2009**No. DOI:10.1002/adma.200803827.
(52) He, C.; Zheng, Z.; Tang, H.; Zhao, L.; Lu, F. *J. Phys. Chem. C* **2009**, *113*, 10322.